

1 Interhemispheric differences in seasonal cycles of tropospheric
2 ozone in the marine boundary layer: observation – model
3 comparisons

4 Richard G. Derwent^{a*}, David D. Parrish^b, Ian E. Galbally^c, David S. Stevenson^d, Ruth M.
5 Doherty^d, Paul J. Young^e, Dudley E. Shallcross^f

6

7 ^a *rdscientific, Newbury, Berkshire, UK*

8 ^b *NOAA ESRL Chemical Sciences Division, 325 Broadway R/CSD7, Boulder, Colorado, USA*

9 ^c *CSIRO Oceans and Atmosphere, PMB1, Aspendale, Victoria 3195, Australia*

10 ^d *School of GeoSciences, The University of Edinburgh, Edinburgh, UK*

11 ^e *Lancaster Environment Centre, Lancaster University, Lancaster, UK.*

12 ^f *Biogeochemistry Research Centre, School of Chemistry, University of Bristol, Bristol, UK.*

13

14 * Corresponding author.

15 *E-mail address: r.derwent@btopenworld.com (R.G.Derwent)*

16

17 Abstract

18 Marine boundary layer ozone seasonal cycles have been quantified by fitting the sum of two
19 sine-curves through monthly detrended observations taken at three stations: Mace Head,
20 Ireland and Trinidad Head, California in the northern hemisphere and Cape Grim, Tasmania
21 in the southern hemisphere. The parameters defining the sine-curve fits at these stations
22 have been compared with those from a global Lagrangian chemistry-transport model
23 (STOCHEM-CRI) and from fourteen ACCMIP chemistry-climate models. Most models
24 substantially overestimated the long-term average ozone levels at Trinidad Head whilst they
25 performed much better for Mace Head and Cape Grim. This led to an underestimation of
26 the observed (North Atlantic inflow – North Pacific inflow) difference. The models generally
27 under-predicted the magnitude of the fundamental term of the fitted seasonal cycle, most
28 strongly at Cape Grim. The models more accurately reproduced the observed second
29 harmonic terms compared to the fundamental terms at all stations. Significant correlations
30 have been identified between the errors in the different models' estimates of the seasonal
31 cycle parameters; these correlations may yield further insights into the causes of the model
32 – measurement discrepancies.

33

34 Key Points

- 35 • Observed and modelled ozone seasonal cycles can be quantified by fitting sine-
36 curves.
- 37 • Models tend to overestimate ozone in northern hemisphere mid-latitude marine
38 boundary layers.
- 39 • Fundamental and second harmonic terms are not always well simulated by models.

40 *Keywords:*

41 Tropospheric ozone, seasonal cycles, ozone production, ozone sinks, interhemispheric
42 differences.

43

44 **1. Introduction**

45 Ozone is widely recognised as an important air pollutant with widespread impacts on
46 human health, crops and vegetation [Monks et al., 2015]. It is the focus of much policy-
47 making activity, the aim of which is to reduce ozone exposures to meet air quality
48 standards, guidelines or criteria by reducing emissions of its precursors, oxides of nitrogen
49 (NO_x) and volatile organic compounds (VOCs). Although many policy questions can be
50 answered using observational networks, models are important tools in the policy
51 formulation process for ozone. Regional-scale chemistry transport or air quality models are
52 in widespread use in the policy-making process to assess and promulgate strategies to
53 achieve satisfactory air quality.

54 As the intensity and frequency of ozone episodes fall in both North America and Europe,
55 there is an increasing focus by policy-makers on the intercontinental transport of ozone by
56 policy-makers [HTAP, 2010; Clifton et al., 2014; Cooper et al., 2015; Doherty, 2015]. In
57 Europe, there are concerns that the progress achieved by the reduction of regional-scale
58 ozone levels has been offset by a growth in the hemispheric ozone levels [Collins et al.,
59 2000] that has been attributed both to anthropogenic and natural (e.g. stratosphere-
60 troposphere exchange, Neu et al. 2014) sources. Although episodic peak ozone levels
61 monitored at the European stations with the highest mean ozone levels have declined
62 markedly since 1980, these episodic peak levels at the stations with the lowest mean ozone
63 have not [Derwent and Hjellbrekke, 2012]. This has been explained by the influence of the
64 hemispheric scale transport of ozone. In North America, global scale chemistry models
65 [Emery et al., 2012; Fiore et al., 2002; Zhang et al., 2011] are utilised to calculate
66 hemispheric scale ozone concentrations transported into regions where exceedances of the
67 United States National Ambient Air Quality Standards (NAAQS) are documented. This is the

68 so-called 'Policy Relevant Background' [US EPA, 2014] or 'North American Background' and
69 further details are given in Lefohn and Cooper, [2015].

70 Whilst the use of regional-scale air quality models in policy formulation is long-standing, the
71 use of global models is relatively recent [HTAP, 2010]. If such models are to provide reliable
72 future guidance for intercontinental policy formulation, then we must have confidence in
73 their performance. Currently, this confidence is established through comparison with
74 observations. However, it has not been possible, so far, to explain the origins of any
75 shortcomings found other than to suspect the adequacy and completeness of any emission
76 inventories employed, as well as chemical mechanisms, boundary layer mixing and
77 convection, deposition, stratosphere-troposphere exchange and lightning [Wild, 2007]. It
78 has not been possible either to reconcile good agreement in one part of the model against
79 poor agreement found elsewhere in these complex models

80 Here we focus on the seasonal cycle in ozone in both models and observations and attempt
81 a detailed examination of both, using techniques that are described in previous work
82 [Parrish et al., 2016]. Our aim is to understand which observed features of the seasonal
83 cycle in ozone are faithfully reproduced by models and which features disagree. Our focus is
84 on the marine boundary layer (MBL) because it receives relatively little in the way of
85 emissions from human activities, because it is isolated from the rest of the troposphere and
86 because it suffers much less from nocturnal depletion under shallow boundary layers. In this
87 way, the process representation in chemistry transport models should be somewhat more
88 reliable compared with that for continental areas. Furthermore, the marine environments
89 upwind of North America and Europe have played an important role in the identification of
90 the global rise in ozone baseline levels and the importance of intercontinental ozone
91 transport [Parrish et al., 2016]. A potential difficulty, however, is the accurate
92 representation in models of the entrainment of ozone-rich free tropospheric air into the
93 MBL.

94 Parrish et al. [2016] compared observed seasonal cycles at eleven MBL sites with the results
95 from three global chemistry-climate models (CCMs). They found similar seasonal cycles
96 between sites within hemispheric scale regions. Here, we consider observations from only
97 three sites that are representative of different hemispheric scale regions, chosen so that
98 there are a pair of stations to reflect the gradient between the northern and southern
99 hemispheres and a pair to reflect North Pacific inflow versus North Atlantic inflow. We
100 compare results across a much larger number of models in order to obtain a more robust
101 evaluation of the abilities of current models to correctly reproduce the seasonal cycle of
102 ozone in the MBL. The models include a global Lagrangian chemistry-transport model
103 STOCHEM-CRI [Derwent et al., 2015], which has increased chemical complexity to treat
104 range of emitted hydrocarbons [Utembe et al., 2010], and the set of fourteen models that
105 took part in the Atmospheric Chemistry Coupled Climate Model Intercomparison Project

106 (ACCMIP) exercise [Young et al., 2013], see the Supplementary Information attached to this
107 paper.

108 **2. Techniques**

109 In this study, seasonal cycles of ozone were defined by least squares fits of sine functions to
110 observed or model monthly mean ozone mixing ratios, as follows:

$$111 \quad y = Y_0 + A_1 \sin(\theta + \phi_1) + A_2 \sin(2\theta + \phi_2) \quad (1)$$

112 where Y_0 is the annual average ozone mixing ratio over the entire set of observations or
113 model results, A_1 and A_2 are amplitudes, ϕ_1 and ϕ_2 are phase angles and θ is a time variable
114 that spans one year's period in 2π radians. The second and third terms on the right hand
115 side of equation (1) are the fundamental and second harmonic terms of the fitted ozone
116 seasonal cycle. In previous work [Parrish et al., 2016], we have shown how the five
117 parameters: Y_0 , A_1 , A_2 , ϕ_1 and ϕ_2 , represented all of the statistically significant information
118 regarding the average seasonal cycle in the observations or model results. The observation –
119 model comparisons in this study are based on the analysis of these five parameters.

120 Full details of the sources of the observations and model results, together with the
121 estimation procedures are given in the Supplementary Information and only a brief
122 summary is given here. Attention was focussed on three marine boundary layer (MBL)
123 baseline stations that have relatively long measurement records: Mace Head, Ireland (1989
124 – 2014) and Trinidad Head, California, United States of America (1990 – 2010) in the
125 northern hemisphere and Cape Grim, Tasmania (1982 - 2010) in the southern hemisphere.
126 The ozone observations employed for Mace Head and Trinidad Head have been carefully
127 filtered to remove local influences but retain baseline levels as described in Parrish et al.,
128 [2016]. In all cases, ozone concentrations are consistently expressed as mixing ratios in
129 units of nmol ozone per mol air, referred to as ppb.

130 Model ozone seasonal cycles were taken from a global Lagrangian chemistry-transport
131 model STOCHEM-CRI and from the set of fourteen chemistry-climate models that took part
132 in the ACCMIP exercise. The model seasonal cycles were based on monthly mean ozone
133 levels, including all hours of the day and night for the lowest model layers of the model grid
134 cells containing the observing stations. The thickness of the lowest model layers and the
135 dimensions of the grid squares containing the three MBL stations varied enormously and no
136 attempt was made to harmonise these differences by interpolation. Uncertainty is
137 introduced into the comparisons discussed below through the spatial mismatch between
138 the observations made at a single point and the model calculations that were effectively an
139 average over single grid cell in the model. This issue for the 3 MBL stations is discussed in
140 some detail in Parrish et al., [2016]. Details of the fourteen models from ACCMIP are given
141 elsewhere [Lamarque et al., 2013; Young et al., 2013].

142 **3. Results**

143 3.1 Observed ozone seasonal cycles

144 The seasonal cycles in ozone at the three selected MBL stations: Mace Head and Trinidad
145 Head in the northern hemisphere and Cape Grim, Tasmania in the southern hemisphere are
146 illustrated in Figure 1 for the observations and the sine-function fits. The annual average
147 ozone mixing ratio for each station has been added to each fitted fundamental curve to
148 facilitate comparison with the observations. The observations and sine-function fits overlap
149 almost exactly at all sites. The fitted curves pass through the 2-sigma confidence limits for
150 each monthly mean at all sites and the root-mean-square deviations between the fits and
151 the monthly means are 0.7, 0.5 and 0.2 ppb for Mace Head, Trinidad Head and Cape Grim,
152 respectively.

153 The observed and fitted seasonal cycles for the northern hemisphere Mace Head and
154 Trinidad Head stations exhibited peaks in April and minima in July to August. The
155 fundamental fits, in contrast, exhibited peaks in early March with minima six months later
156 (September). The second harmonic fit showed two peaks, one in April and the other six
157 months later (October). The observed and fitted seasonal cycles for the southern
158 hemisphere Cape Grim station peaked in August and showed a minimum in January. The
159 fundamental fit for Cape Grim exhibited a peak in August. The second harmonic fit showed
160 the same two peaks as in the northern hemisphere (April and October).

161 In this manner, it has been possible to quantify using five parameters: Y_0 , A_1 , ϕ_1 , A_2 and ϕ_2 ,
162 the observed seasonal cycles for the three MBL stations without loss of features and details
163 or distortions. The fitted parameters and their confidence limits are presented in the
164 Supplementary Information. Notably, all parameters derived here from the observations at
165 the three stations are consistent with the values reported in Table 2 of Parrish et al., [2016];
166 comparison of future model results can simply use these tabulated values without directly
167 accessing and analysing the monthly mean data themselves. An examination of model
168 seasonal cycles now follows using the same sine-curve fitting procedures.

169 3.2 Comparison of the observed and modelled seasonal cycles

170 In this section, the fitted sine-curves to the seasonal cycles in the observations and models
171 are compared using the five parameters: Y_0 , A_1 , ϕ_1 , A_2 and ϕ_2 , defined above in equation (1).
172 The aim is to ascertain how well the models are able to quantify the seasonal cycles across
173 the three MBL stations which have been chosen so that there are a pair of stations to reflect
174 the gradient between the northern hemisphere versus the southern hemisphere and a pair
175 to reflect North Pacific Ocean inflow versus North Atlantic Ocean inflow. Bar graphs of the
176 observations and model ACCMIP ensemble mean (ENSEMBLE) results, with the STOCHEM-
177 CRI and individual ACCMIP member results included as points are used to examine whether
178 the models are able to account for the range in the observed seasonal cycle parameters
179 between the three MBL stations. The detailed values of all parameters are tabulated in the
180 Supplementary Information.

181 3.2.1 Long-term average ozone levels, Y_0

182 The long-term average ozone levels, Y_0 , are compared at the three MBL stations in Figure 2.
183 The observed values of Y_0 were, in ascending order: Cape Grim, 25.0 ± 0.2 ppb; Trinidad
184 Head, 32.0 ± 0.7 ppb and Mace Head, 38.9 ± 0.4 , where the quoted uncertainty ranges are 2
185 $-\sigma$ or 95% confidence limits. All the models gave Cape Grim the lowest Y_0 but they
186 disagreed about which station had the highest Y_0 . The models typically show: Cape Grim <
187 Mace Head < Trinidad Head. Further, Figure 2 shows that the models overestimate the
188 observations for the Trinidad Head station by 2 to 19 ppb and that this discrepancy is the
189 largest among the three stations.

190 The STOCHEM-CRI model calculated Y_0 values in the order: Cape Grim, 28.1 ± 0.8 ppb; Mace
191 Head, 32.3 ± 2.1 ppb and Trinidad Head, 35.0 ± 1.8 ppb, respectively which gave the
192 incorrect order for the North Pacific – inflow versus the North Atlantic – inflow stations. A
193 similar problem was found for the ACCMIP models, with the predicted Y_0 values for the
194 ENSEMBLE: Cape Grim, 24.4 ± 0.2 ppb; Mace Head, 40.8 ± 0.3 ppb and Trinidad Head, $41.1 \pm$
195 0.2 ppb. If account were taken of the 2 $-\sigma$ error bars, then STOCHEM-CRI and the ACCMIP-
196 ENSEMBLE both gave Mace Head minus – Trinidad Head differences that were statistically
197 indistinguishable from zero. In contrast, the observed Mace Head – Trinidad Head
198 differences were highly statistically significant, 6.8 ± 0.8 ppb. This difference was first
199 recognised by Parrish et al. [2009] who reported 7 ± 2 ppb higher ozone in all seasons
200 arriving at European baseline stations versus those in North America, in close agreement
201 with the current estimate. Parrish et al. [2009] could not provide an explanation for this
202 difference, and none of the models was able to reproduce it.

203 Using tagged tracers in the STOCHEM-CRI model [Derwent et al., 2015], the Y_0 value for
204 ozone undergoing intercontinental transport to Trinidad Head was 24.8 ± 1.6 ppb compared
205 with 35.0 ± 1.8 ppb for ozone from all sources. The corresponding STOCHEM-CRI Y_0 values
206 for Mace Head were 29.7 ± 2.2 ppb and 32.3 ± 2.1 ppb, which suggested a smaller local
207 ozone contribution than for Trinidad Head. This difference in behaviour suggested a larger
208 local North American contribution at Trinidad Head compared with the local European
209 contribution at Mace Head in the STOCHEM-CRI chemistry transport model.

210 Of the 14 ACCMIP models, only one model in addition to STOCHEM-CRI (see Figure 2) gave a
211 Y_0 value for Trinidad Head that fell within $\pm 10\%$ of the observations. The remaining 13
212 models gave substantially larger Y_0 values. This left the ENSEMBLE average substantially
213 larger also. For Mace Head, the ACCMIP models performed much better such that several
214 models and the ENSEMBLE gave results that fell within $\pm 10\%$. However, the Mace Head –
215 Trinidad Head differences were found to lie within the range from -3.21 to +6.83 ppb, with
216 the ENSEMBLE at -0.33 ppb. These should be compared with the observed difference of $+6.8$
217 ± 0.8 ppb. Only one of the ACCMIP models gave a reasonable estimate of the Mace Head –
218 Trinidad Head difference of +6.83 ppb, but then only by overestimating both Y_0 values by
219 substantial amounts, of the order of 7 ppb.

220 3.2.2 Amplitudes of the fundamental, A_1

221 The detailed values of A_1 are shown on the left side of Figure 3. The observed amplitudes of
222 the fundamentals, A_1 , were found to be: Mace Head, 5.6 ± 0.6 ppb; Trinidad Head, 5.7 ± 0.9
223 ppb and Cape Grim, 7.1 ± 0.2 ppb. The A_1 values for the two northern hemisphere stations
224 were statistically indistinguishable, with that for the southern hemisphere station
225 significantly greater. The observed order of the stations was therefore: Mace Head \approx
226 Trinidad Head < Cape Grim.

227 Model performance for this parameter was generally poor. STOCHEM-CRI gave reasonable
228 estimates for A_1 at Mace Head, 4.7 ± 3.0 ppb and Cape Grim, 8.2 ± 1.2 ppb but that for
229 Trinidad Head was too low by a wide margin, 2.8 ± 2.6 ppb. The results for this model were
230 outside the $\pm 10\%$ range and the stations were ordered differently than the observations:
231 Trinidad Head < Mace Head < Cape Grim.

232 Agreement for the amplitudes from the ACCMIP models was also poor overall. The
233 ENSEMBLE gave its lowest A_1 value for Cape Grim, 2.9 ± 0.2 ppb, next highest for Trinidad
234 Head, 3.4 ± 0.2 ppb and highest for Mace Head, 4.1 ± 0.4 ppb. Again, the stations were
235 ordered differently than the observations: Cape Grim < Trinidad Head < Mace Head. Of all
236 the ACCMIP models, only one gave an A_1 value for Mace Head within $\pm 10\%$ of the observed
237 and one (though not the same model) for Trinidad Head. There were no ACCMIP predictions
238 of A_1 within $\pm 10\%$ of that observed for Cape Grim because generally all simulated
239 amplitudes were gross underestimations, see Figure 3.

240 The northern Hemisphere – southern Hemisphere difference as indexed by the Mace Head –
241 Cape Grim difference was found to be -1.5 ± 0.6 ppb in the observations. This difference was
242 reported to be -3.5 ± 1.6 ppb in STOCHEM-CRI which, although it was of the correct sign,
243 was found to be a substantially overestimated, as shown by the gradients in Figure 3. The
244 ACCMIP ENSEMBLE gave a difference of $+1.2 \pm 0.4$ ppb, which although approximately of
245 the correct magnitude, had the incorrect sign.

246 STOCHEM-CRI and most ACCMIP models underestimated the A_1 values for the Trinidad
247 Head station. When taken with the overestimation problem with the Y_0 values for the same
248 station described in section 3.2.1 above, the underestimation problem with the A_1 values
249 may point to a common issue across the models.

250 The ACCMIP models also performed poorly for Cape Grim but, in contrast, STOCHEM-CRI
251 performed well at this station. The ACCMIP models significantly underestimated the
252 strength of the fundamental amplitude of the seasonal cycle at Cape Grim compared with
253 the observations. Whereas a marked seasonal cycle was observed, little was predicted. This
254 may point to an underestimation by all models of photochemical ozone destruction or an
255 overestimation of photochemical ozone production during the Austral summer.

256 3.2.3 Phase angles of the fundamental, ϕ_1

257 To facilitate comparison of the phase angles of the fundamentals of the observations and
258 models between the northern and southern hemispheres, northern hemisphere ϕ_1 values
259 have been shifted by $-\pi$ radians when plotted in Figure 4 and discussed below. With this
260 adjustment, fundamental phase angles overlapped corresponding to a spring maxima in
261 both hemispheres in both observations and models. ϕ_1 values were found to be less
262 negative (peak earlier in the spring) for the observations at Cape Grim, -2.10 ± 0.03 radians,
263 and more negative (peak later in the spring) at the two northern hemisphere stations:
264 Trinidad Head, -2.66 ± 0.16 radians, and Mace Head, -2.63 ± 0.06 radians. The two northern
265 hemisphere stations had ϕ_1 values that were statistically indistinguishable. The average
266 observed difference in ϕ_1 between the hemispheres (-0.54 ± 0.16 radians or 31 ± 9 days)
267 indicated that the maximum of the fundamental term occurred one month later in the
268 northern hemisphere compared with the southern hemisphere. This difference may reflect
269 the greater importance of photochemical ozone production in the northern hemisphere
270 where the large majority of man-made ozone precursors are emitted.

271 The ACCMIP ENSEMBLE values of ϕ_1 for the three stations gave the same overall pattern as
272 the observations, see Figure 4, with Cape Grim as less negative and the two northern
273 hemisphere stations as more negative, that is to say, earlier and later spring maxima,
274 respectively. The observed phases of all stations were well reproduced by the ACCMIP
275 ENSEMBLE but the models exhibited substantial variability that was larger in the northern
276 hemisphere. One of the ACCMIP models exhibited a phase angle at Trinidad Head that was
277 up to 2.5 radians (5 months) later in the year compared with the observations. The
278 STOCHEM-CRI model did not accurately reproduce that phase at any station and was nearly
279 completely out of phase at Mace Head.

280 3.2.4 Amplitudes of the second harmonics, A_2

281 The amplitudes of the second harmonics in the observations showed a regular progression
282 across the three MBL stations (Figure 3): Cape Grim, 1.7 ± 0.2 ppb; Mace Head, 3.0 ± 0.6 ppb
283 and Trinidad Head, 3.5 ± 0.9 ppb.

284 Figure 3 demonstrates that the models have significant skill in reproducing the broad spatial
285 pattern in the observed second harmonic amplitudes. The amplitudes of the second
286 harmonic in the STOCHEM-CRI model were found within $\pm 10\%$ for Cape Grim and Mace
287 Head but overestimated the observed value for Trinidad Head by 45%. The ACCMIP
288 ENSEMBLE indicated a steeper gradient across the three MBL stations, underestimating the
289 observed second harmonic amplitude at Cape Grim by more than a factor of two and
290 overestimating it at Trinidad Head by 25%.

291 A substantial number of the ACCMIP models gave second harmonic amplitudes that lay
292 within $\pm 10\%$. However, it was not always the same ACCMIP members that performed well
293 at each station. There was significant variability in the ACCMIP results, such that the

294 amplitudes spanned nearly a factor of three from 2.7 to 7.8 ppb at Trinidad Head, from 2.0
295 to 7.2 ppb at Mace Head and from 0.1 to 2.5 ppb at Cape Grim.

296 On the whole, the ACCMIP models reproduced the amplitude of the second harmonic better
297 than that of the fundamental. Figure 3 shows closer accord of the absolute magnitudes for
298 the ACCMIP ENSEMBLE for A_2 than for A_1 and the standard deviations of the ACCMIP
299 members are smaller for A_2 than A_1 .

300 3.2.5 Phase angles of the second harmonics, ϕ_2

301 The phase angles of the second harmonics are presented in Figure 4, noting that no shifting
302 by $-\pi$ radians has been applied to the northern hemisphere stations as with ϕ_1 . The
303 observed order of the ϕ_2 values was: Mace Head \approx Trinidad Head and both more negative
304 than Cape Grim with the phase angles of the two northern hemisphere stations statistically
305 indistinguishable: Mace Head, -2.4 ± 0.2 radians and Trinidad Head, -2.3 ± 0.3 radians. The
306 observed difference in phase angle between the northern hemisphere versus the southern
307 hemisphere stations was small but statistically significant at -0.6 ± 0.3 radians (16 ± 8 days
308 later maxima in the northern hemisphere).

309 The ACCMIP ENSEMBLE estimated ϕ_2 values at Mace Head and Cape Grim with pinpoint
310 accuracy, within 0.07 radians or 2 days but was 0.37 ± 0.03 radians less negative or 11 ± 1
311 days earlier at Trinidad Head. The ACCMIP ENSEMBLE was thus able to accurately reproduce
312 the observed difference in phase angle between Mace Head in the northern and Cape Grim
313 in the southern hemisphere (-0.46 ± 0.3 radians). STOCHEM-CRI accurately reproduced the
314 observed ϕ_2 values at Cape Grim but was 0.44 ± 0.26 radians or 13 ± 8 days early at Trinidad
315 Head. However, this model was a long way out at Mace Head for this parameter.

316 There was a large range in the estimated second harmonic phase angles between the
317 individual ACCMIP members, however. The northern hemisphere stations exhibited ϕ_2
318 values between -3.2 and -1.3 radians (23 days later to 30 days earlier) and the southern
319 hemisphere values ranged between -3.2 and 1.2 radians (41 days later to 85 days earlier)
320 relative to the observations.

321 In accord with the behaviour found for the amplitudes, the ACCMIP models reproduced the
322 phase of the second harmonic better than that of the fundamental. Figure 4 shows good
323 agreement on average for both phase angles but the standard deviations of the ACCMIP
324 members are smaller for ϕ_1 than for ϕ_2 . This is even more pronounced when the variability
325 is considered in days compared to radians.

326 3.2.6 Variations in interhemispheric differences between the ACCMIP models

327 Direct examination of the interhemispheric differences can provide additional information
328 that is not apparent from examination of model – observation differences at the separate
329 stations. Figure 5 shows the interhemispheric differences for the five parameters discussed

330 in the preceding sections. They are plotted between the northern and southern hemisphere
331 (NS), calculated from Trinidad Head and Cape Grim parameters, and between the Atlantic
332 and Pacific (AP) inflow stations, calculated from the Mace Head and Trinidad Head
333 parameters. In Figure 5, the standard deviations of the results of the fourteen ACCMIP
334 members are annotated. A striking feature of these standard deviations is that in most cases
335 the standard deviations of the differences are smaller than the standard deviations at the
336 individual stations annotated in Figures 2-4. Propagation of error considerations lead to the
337 expectation of larger standard deviations for the differences if the model errors at the
338 individual stations are uncorrelated. Therefore, this feature indicates that the model errors
339 are significantly correlated between the stations.

340 The correlation of the Y_0 parameters derived from the separate ACCMIP members is
341 examined in Figure 6a. The Y_0 values are highly correlated between Mace Head and Trinidad
342 Head ($r^2 = 0.74$). This correlation indicates that, in addition to an overall bias between Mace
343 Head and Trinidad Head, each ACCMIP member tends to further overestimate Y_0 at both of
344 these northern hemisphere mid-latitude stations by a similar amount, although the
345 magnitude of this overestimation varies between the models. The correlation of the Y_0
346 values between Cape Grim and Trinidad Head is much poorer ($r^2 = 0.15$) with the ACCMIP
347 models accurately reproducing the Cape Grim values, on average. A general positive bias of
348 Chemistry-Climate Models for lower tropospheric ozone has been discussed [e.g. Lamarque
349 et al., 2012; Naik et al., 2013; Parrish et al., 2014]; however, the correlations in Figure 6a
350 suggest that such overestimates are found in all of the ACCMIP members at northern mid-
351 latitudes, but are not a general global feature. Young et al. [2013] and Parrish et al., [2016]
352 also found model overestimates at northern but not southern mid-latitudes. If the bias is
353 indeed limited to northern mid-latitudes, this regional difference may help to diagnose the
354 cause of the problem. In this case, the problem could arise from model treatment of
355 anthropogenic emissions (which are concentrated at northern mid-latitudes) or model
356 treatment of ozone deposition to continental surfaces (which are also concentrated in that
357 region) or potential “dynamic” influences (weather patterns tend to be more complex and
358 variable due to the more pronounced land-sea contrasts).

359 The correlations for all five parameters derived from the separate ACCMIP members are
360 compared for NS and AP in Figure 6b and the correlation plots for amplitudes and phase
361 angles are included in the Supplementary Material (Figures S1 and S2). The magnitudes of
362 the fundamental of the seasonal cycles (A_1) are significantly correlated between Mace Head
363 and Trinidad Head ($r^2 = 0.58$) and between Cape Grim and Trinidad Head ($r^2 = 0.48$). These
364 correlations indicate that about one-half of the variance between the different models and
365 between the models and the measurements is due to problems within each model that are
366 common to all three sites, and the other half of the variance is due to model problems that
367 differ between sites.

368

369 The errors for the ACCMIP members are significantly correlated for most of these
370 parameters for both the NS and AP comparisons. These correlations all indicate that the
371 ACCMIP models differ in important respects in their treatment of the processes that drive
372 the ozone seasonal cycle throughout the troposphere, and the correlations can potentially
373 provide diagnostic information regarding the causes of the errors within the individual
374 ACCMIP models. One difficulty with such diagnosis is the limited precision possible for the
375 determination of the seasonal cycle parameters with only a few years (5 to 10 years for the
376 ACCMIP models and a single year for the STOCHEM-CRI model) of model simulations; the
377 confidence limits of these parameter determinations (Tables S1 – S3) are of the order of the
378 model – measurement differences, which limits our ability to interpret the present results.
379 Future examination of the correlations with improved precision could provide useful
380 guidance for model improvement.

381 **4. Discussion and conclusions**

382 To understand the seasonal cycle of ozone in the MBL, a simple conceptual model has been
383 employed as formulated in our previous study [Parrish et al., 2016] in which ozone
384 produced photochemically in the free troposphere or in the continental polluted boundary
385 layer or injected from the stratosphere is entrained into or advected into the MBL. The late
386 winter to early spring maximum and the corresponding late summer minimum is a reflection
387 of the domination of the ozone seasonal cycle by net photochemical destruction in the MBL
388 [Ayers et al., 1992; Oltmans and Levy, 1994]. Faster destruction in summer versus winter
389 accounts for the summertime minimum and wintertime maximum. Consequently, ozone
390 maximises in late winter to early spring and this is the main driver of the fundamental
391 harmonic term seen in Figure 1 at the three chosen MBL stations. There may also be
392 contributions from seasonal cycles in the entrainment of ozone-rich free tropospheric air
393 into the MBL. The observed seasonal cycles are not pure sine curves and there is evidence
394 for secondary maxima in late autumn and ‘shoulders’ during the late winter, see Figure 1.
395 This behaviour is reflected in a large contribution from the second harmonic term as
396 described by Parrish et al., [2016] who first recognised and quantified this term which they
397 found to be a robust feature of observations and models for MBL stations. They argued that
398 the second harmonic resulted from a second harmonic in the seasonal cycle of the
399 photolysis rate coefficient of ozone which acts as the main photochemical destruction sink
400 for ozone and provided a detailed discussion of this issue (see Section 4.3 of Parrish et al.,
401 [2016]).

402 In this study, we have extended the Parrish et al., [2016] work by analysing the seasonal
403 cycles of 14 ACCMIP models rather than the three models of Parrish et al., [2016], together
404 with the STOCHEM-CRI model at three MBL stations: Mace Head, Trinidad Head and Cape
405 Grim. These three stations allowed us to focus on interhemispheric differences, that is to
406 say, northern versus southern hemisphere and North Pacific versus North Atlantic. Our main
407 finding was that we could accurately describe the seasonal cycles in the observations and all

408 model results by fitting sine-curves and deriving five parameters: Y_0 , A_1 , ϕ_1 , A_2 and ϕ_2 in
409 equation (1). The fundamental term: $A_1 \sin(\theta + \phi_1)$, described the majority of the seasonal
410 variations in both observed and modelled ozone. However, a second harmonic term of the
411 form: $A_2 \sin(2\theta + \phi_2)$, was required to generate an accurate fit to all sets of observations and
412 model results. Together, the five parameters provided a convenient means of accurately
413 quantifying observed and model seasonal cycles.

414 Armed with this analytical tool, a systematic assessment was made of the seasonal cycles
415 produced by STOCHEM-CRI and the 14 ACCMIP members and their ensemble mean
416 (ENSEMBLE). Compared to the fundamental, all models more accurately reproduced the
417 observed second harmonic terms. This accurate agreement both in amplitude and phase
418 angle suggested that the second harmonic term arose from a cyclic phenomenon that was
419 well simulated by all models. The cycle of the actinic flux and its control of the
420 photochemical destruction of ozone, is a strong candidate to explain the second harmonic
421 term, as argued by Parrish et al., [2016]. However, despite the general agreement found
422 between the observed and model terms: A_2 and ϕ_2 , there was a large amount of variability
423 between the results from the different ACCMIP members. The representation of the
424 photochemical destruction sink for ozone should be straight-forwardly represented in the
425 ACCMIP models and it is not at all clear why there should be such large variability. Further
426 analysis was beyond the scope of this study.

427 Despite the large increase in chemical complexity in STOCHEM-CRI compared with the
428 ACCMIP models, there did not appear to be much improvement in performance for the
429 second harmonic parameters: A_2 and ϕ_2 , versus observations. The STOCHEM-CRI and
430 ACCMIP ENSEMBLE values for A_2 agreed reasonably closely, except for Cape Grim, and those
431 for ϕ_2 , except for Trinidad Head. The increase in chemical complexity in STOCHEM-CRI was
432 entirely in the photochemical processes leading to ozone production. Because there was
433 little or no increase in the complexity of the ozone destruction processes, it was reasonable
434 that the second harmonic terms should be similar, assuming a similar level of treatment of
435 the solar actinic fluxes. There was no significant improvement in the performance of
436 STOCHEM-CRI with respect to A_1 and ϕ_1 compared to the ACCMIP models, for reasons
437 which are not clear without further detailed information of the formulation of the ACCMIP
438 models.

439 The model treatments of the fundamental terms: $A_1 \sin(\theta + \phi_1)$ and of the individual
440 parameters: A_1 and ϕ_1 , were in many cases in poor agreement with those of the
441 observations. STOCHEM-CRI reproduced the observed fundamental amplitudes well at
442 Mace Head and Cape Grim but underestimated them at Trinidad Head. The ACCMIP
443 ENSEMBLE only performed well at Mace Head, in contrast, underestimating A_1 at the other
444 stations. The ACCMIP ENSEMBLE performed well for ϕ_2 at all stations in contrast to
445 STOCHEM-CRI which only performed well at Mace Head.

446 Further work is required to work through the model discrepancies found here to ascertain
447 candidate explanations and identify needed improvements in tropospheric ozone models.
448 We have identified those features of the model seasonal cycles that appear to be
449 reasonably well described, namely the photochemical ozone sinks. Entrainment of free
450 tropospheric air is expected to be an important factor controlling the concentrations and
451 seasonality of MBL ozone; it will be important to investigate model treatment of this
452 entrainment and degree of isolation of the MBL. We have also identified a particularly large
453 extent of variability in the simulated ozone seasonal cycles between the ACCMIP members.
454 Detailed analysis of ozone budget terms (including, for example, the possible importance of
455 halogen chemistry) will be required over and above that already performed by Young et al.,
456 [2013] before the causes of the model variability and detailed discrepancies can be
457 established. We have also identified significant correlations between the parameters
458 derived from the individual ACCMIP models. For example, the models generally
459 overestimate the long-term average ozone levels (Y_0) at northern mid-latitudes (but not in
460 the southern hemisphere) and the overestimates of the different ACCMIP members
461 correlate between Mace Head and Trinidad Head, possibly suggesting a model difficulty in
462 treating anthropogenic emissions or surface deposition, and that this difficulty varies
463 between models. Model errors in A_1 correlate between all three stations, while model
464 errors in A_2 and ϕ_1 correlate between Mace Head and Trinidad Head, but not between the
465 northern and southern hemispheres. We suggest that future work further investigating
466 these correlations in more detail may yield further insights into the causes of model-
467 measurement discrepancies. Until these issues can be resolved, large uncertainties remain
468 in tropospheric model simulations of ozone transported on intercontinental scales.

469 **Acknowledgements**

470 The authors are grateful to P.G. Simmonds and T.G. Spain for providing the Mace Head data
471 and for A.J. Manning for sorting the Mace Head data into baseline and non-baseline
472 observations. The data analysed here are available from the sources cited in the
473 Supplementary Information.

474 D. Parrish acknowledges support from NOAA's Climate Program Office.

475 R. Derwent acknowledges support from the Department for Energy and Climate Change UK,
476 under contract CESA 002 and from Department for Environment, Food and Rural Affairs UK
477 for the development of STOCHEM and the CRI mechanism.

478 P. J. Young acknowledges support by an Early Career Integration Grant from Lancaster
479 University.

480 **References**

481 Ayers, G.P., S.A. Penkett, R.W. Gillett, B. Bandy, I.E. Galbally, C.P. Meyer, C.M. Elsworth, S.T.
482 Bentley, and B.W. Forgan (1992). Evidence for photochemical control of ozone
483 concentrations in unpolluted marine air. *Nature* 360, 446-449.

484 Clifton, O.E., A.M. Fiore, G. Correa, L.W. Horowitz, and V. Naik (2014). Twenty-first century
485 reversal of the surface ozone seasonal cycle over the north-eastern United States.
486 *Geophysical Research Letters* 41, 7343-7350, doi:10.1012/2014GL061378.

487 Collins, W.J., D.S. Stevenson, C.E. Johnson, and R.G. Derwent (1997). Tropospheric ozone in
488 a Global-Scale Three-Dimensional Lagrangian Model and its response to NO_x emission
489 controls. *Journal of Atmospheric Chemistry* 26, 223-274.

490 Collins, W.J., D.S. Stevenson, C.E. Johnson, and R.G. Derwent (2000). The European regional
491 ozone distribution and its links with the global scale for the years 1992 and 2015.
492 *Atmospheric Environment* 34, 255-267.

493 Cooper, O.R., A.O. Langford, D.D. Parrish, and D.W. Fahey (2015) Challenges of a lowered
494 U.S. ozone standard, *Science*, 348(6239), 1096-1097, doi:10.1126/science.aaa5748.

495 Derwent, R.G., and A.-G. Hjellbrekke (2012). Air pollution by ozone across Europe.
496 *Handbook on Environmental Chemistry*, 163. Springer-Verlag, Berlin.

497 Derwent, R.G., A.J. Manning, P.G. Simmonds, P.G., and T.G. Spain (2013). Analysis and
498 interpretation of 25 years of ozone observations at the Mace Head Atmospheric Research
499 Station on the Atlantic Ocean coast of Ireland from 1987 to 2012. *Atmospheric Environment*
500 80, 361-368.

501 Derwent, R.G., S.R. Utembe, M.E. Jenkin, and D.E., Shallcross (2015). Tropospheric ozone
502 production regions and the intercontinental origins of surface ozone over Europe.
503 *Atmospheric Environment* 112, 216-224.

504 Doherty, R.M. (2015). Ozone pollution from near and far. *Nature Geoscience, News and*
505 *Views*, 10th August.

506 Emery, C., J. Jung, N. Downey, J. Johnson, M. Jimenez, G. Yarwood, and R. Morris (2012).
507 Regional and global model estimates of policy relevant background ozone over the United
508 States. *Atmospheric Environment* 47, 206-217.

509 Fiore, A.M., D.J. Jacob, I. Bey, R.M. Yantosca, B.D. Field, and A.C. Fusco (2002). Background
510 ozone over the United States in summer: Origin, trend and contribution to pollution
511 episodes. *Journal of Geophysical Research* 107, D4275, doi: 10.1029/2001JD000982.

512 HTAP (2010). Hemispheric transport of air pollution 2010. Part A.: ozone and particulate
513 matter. *Air Pollution Studies No. 17*. United Nations, Geneva, Switzerland.

514 Jenkin, M.E., L.A. Watson, S.R. Utembe, and D.E. Shallcross (2008). A Common
515 Representative Intermediate (CRI) mechanism for VOC degradation. Part-1: gas phase
516 mechanism development. *Atmospheric Environment* 42, 7185-7195.

517 Lamarque, J. F., et al. (2012). CAM-chem: description and evaluation of interactive
518 atmospheric chemistry in the Community Earth System Model. *Geosci. Model Dev.*, 5, 369-
519 411, doi:10.5194/gmd-5-369-2012.

520 Lamarque, J.F., et al. (2013). The Atmospheric Chemistry and Climate Model
521 Intercomparison Project (ACCMIP): overview and description of models, simulations and
522 climate diagnostics. *Geoscientific Model Development* 6, 179-206.
523 <http://doi.org/10.5194/gmd-6-179-2013>.

524 Lefohn, A.S., and O.R. Cooper (2015). Introduction to the special issue on observations and
525 source attribution of ozone in rural regions of the western United States. *Atmospheric*
526 *Environment* 109, 279-281.

527 Monks, P.S., et al. (2015). Tropospheric ozone and its precursors from the urban to the
528 global scale from air quality to short-lived climate forcer. *Atmospheric Chemistry and*
529 *Physics* 15, 8889-8973.

530 Naik, V., et al. (2013). Pre-industrial to present-day changes in tropospheric hydroxyl and
531 methane lifetime from the Atmospheric Chemistry and Climate Model Intercomparison
532 Project (ACCMIP). *Atmospheric Chemistry and Physics* 13, 5277-5298.

533 Naik, V., L. W. Horowitz, A. M. Fiore, P. Ginoux, J. Mao, A. M. Aghedo, and H. Levy (2013).
534 Impact of preindustrial to present-day changes in short-lived pollutant emissions on
535 atmospheric composition and climate forcing. *J. Geophys. Res.*, 118,
536 doi:10.1002/jgrd.50608.

537 Neu et al., Tropospheric ozone variations governed by changes in stratospheric circulation
538 *Nature Geoscience* 7, 340–344 (2014) doi:10.1038/ngeo2138.

539 Oltmans, S.J., and H. Levy (1994). Surface ozone measurements from a global network.
540 *Atmospheric Environment* 28, 9-24.

541 Parrish, D.D., D.B. Miller, and A.H. Goldstein, (2009). Increasing ozone in marine boundary
542 layer inflow at the west coasts of North America and Europe. *Atmospheric Chemistry and*
543 *Physics* 9, 1303-1323.

544 Parrish, D.D., et al. (2014). Long-term changes in lower tropospheric baseline ozone
545 concentrations: Comparing chemistry-climate models and observations at northern mid-
546 latitudes. *J. Geophys. Res.*, 119, doi:10.1002/ 2013JD021435.

547 Parrish, D.D., et al. (2016). Seasonal cycles of O₃ in the marine boundary layer: Observation
548 and model simulation comparisons. *Journal of Geophysical Research: Atmospheres* 121,
549 doi:10.1002/2015JD024101.

550 Sherrod, P.H. (1992). NLREG: Non-linear regression software. <http://www.nlreg.com>.

551 US EPA (2014). Policy assessment for the review of the ozone National Ambient Air Quality
552 Standards. United States Environmental Protection Agency EPA-425/R-14-006, US EPA,
553 Research Triangle Park, North Carolina.

554 Utembe, S.R., et al. (2010). Using a reduced Common Representative Intermediates (CRIv2-
555 R5) mechanism to simulate tropospheric ozone in a 3-D Lagrangian chemistry transport
556 model. *Atmospheric Environment* 44, 1609-1622.

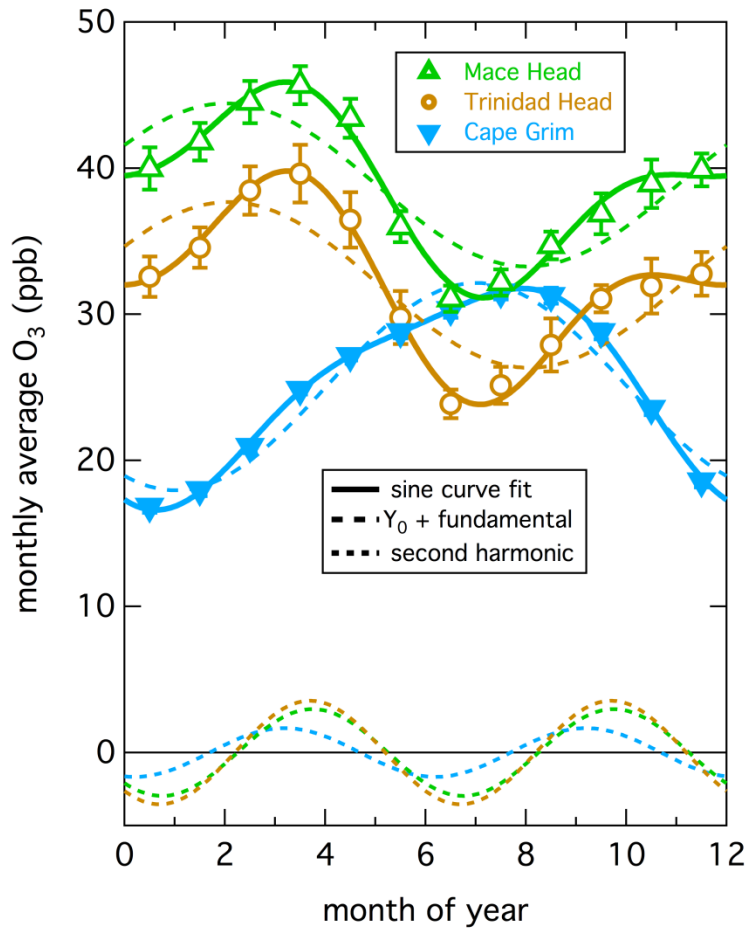
557 Wild, O. (2007). Modelling the global tropospheric ozone budget: exploring the variability in
558 current models. *Atmospheric Chemistry and Physics* 7, 2643-2660.

559 Young, P. J., et al. (2013). Pre-industrial to end 21st century projections of tropospheric
560 ozone from the Atmospheric Chemistry and Climate Model Intercomparison Project.
561 *Atmospheric Chemistry and Physics* 13, 2063-2090.

562 Zhang, L., et al. (2011). Improved estimates of the policy-relevant background ozone in the
563 United States using the GEOS-Chem global model with 1/2° x 2/3° horizontal resolution over
564 North America. *Atmospheric Environment* 45, 6769-6776.

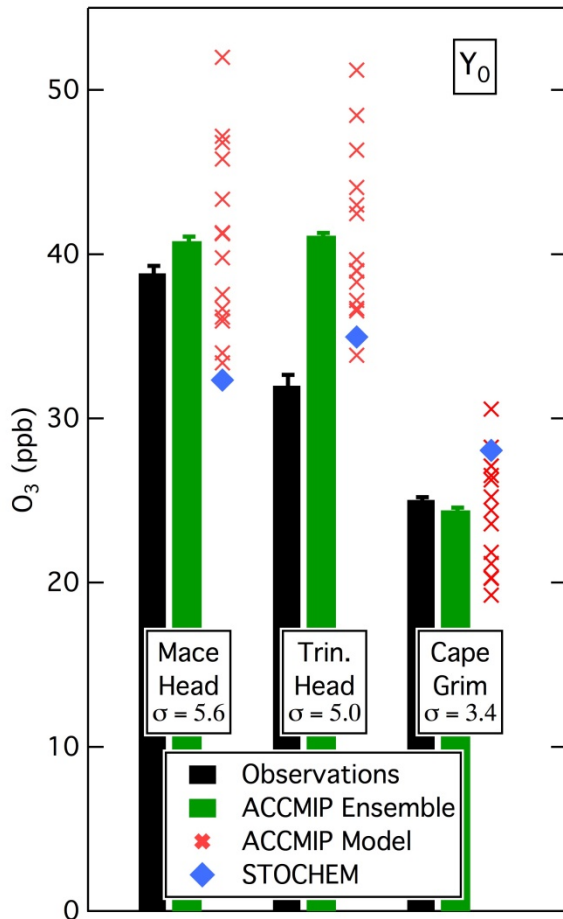
565

566



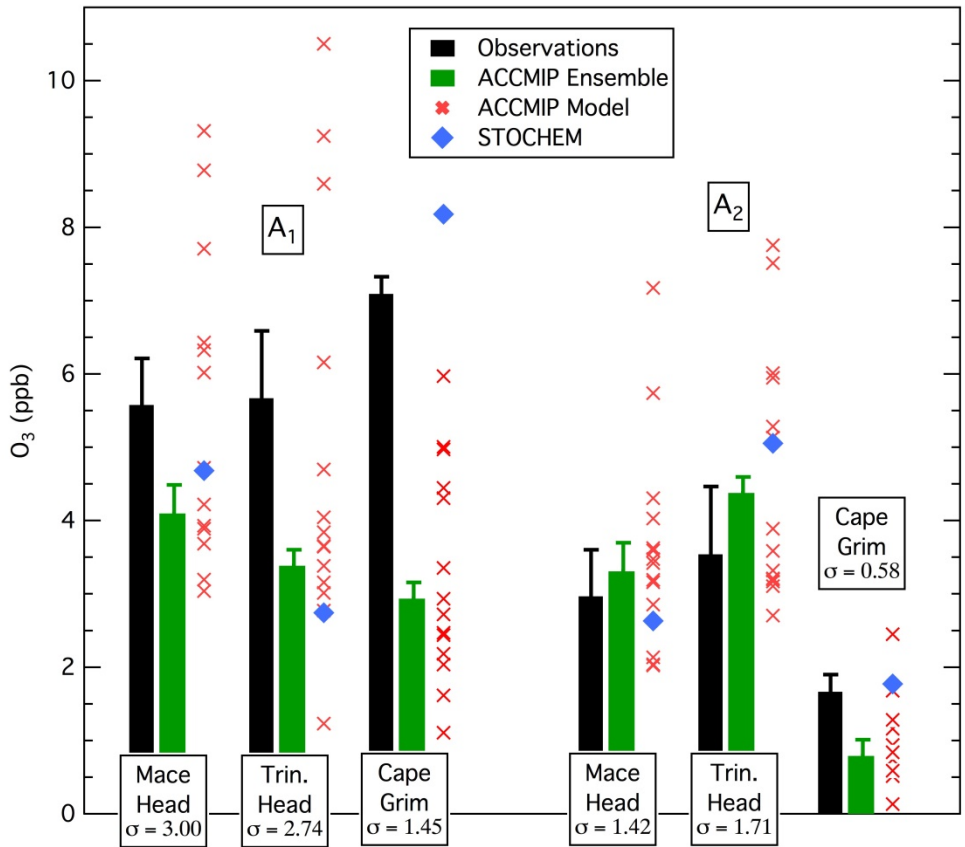
567

568 **Figure 1.** Sine-curve fitted ozone seasonal cycles (solid lines) to observations from Mace
 569 Head, Ireland (26 years), Trinidad Head, California (21 years) and Cape Grim, Tasmania (29
 570 years), together with the fundamental and second harmonic fits (dashed lines). The
 571 symbols give average monthly ozone concentrations over the entire data records with error
 572 bars indicating 2-sigma confidence limits (some error bars are obscured by the size of the
 573 symbols).



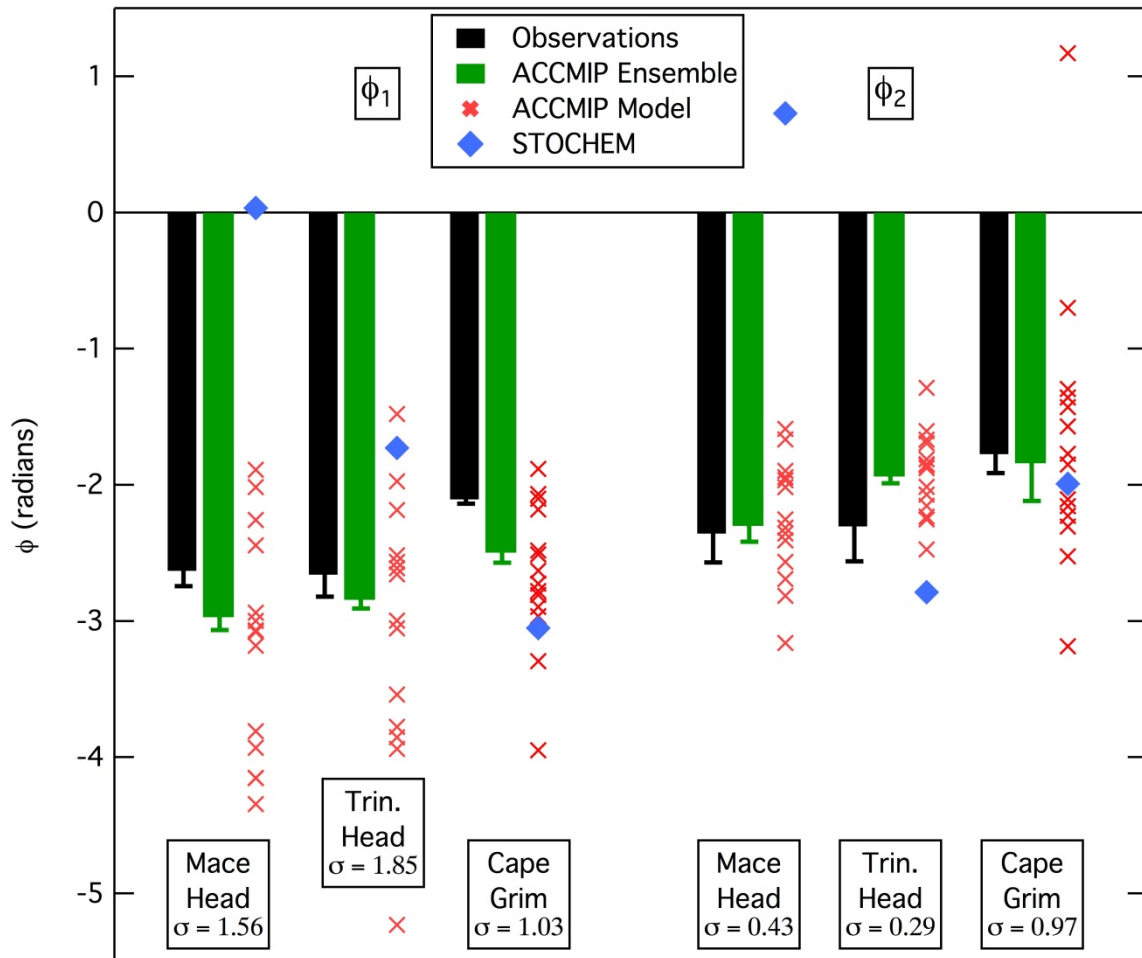
574

575 **Figure 2.** Comparison of the observed and model values of the average ozone mixing ratio
 576 over the entire dataset, Y_0 , in ppb for the STOICHEM-CRI model, the ACCMIP members and
 577 their ENSEMBLE. Error bars indicate 2-sigma confidence limits for the observations and
 578 ACCMIP ensemble. The standard deviations of the results of the ACCMIP members are
 579 annotated for the three sites.



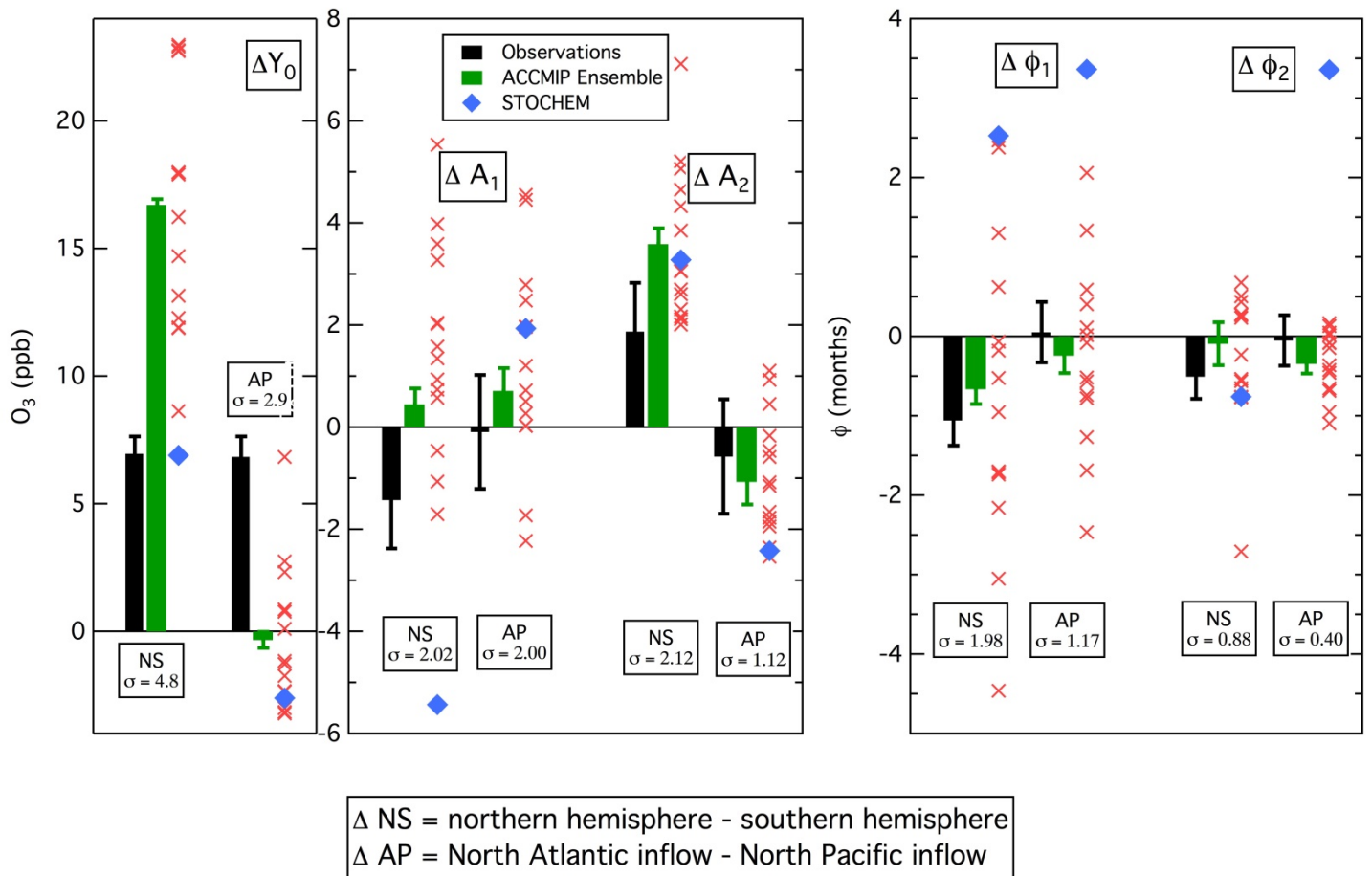
580

581 **Figure 3.** Comparison of the observed and model values of the fundamental and second
 582 harmonic amplitudes, A₁ and A₂, in ppb for the STOICHEM-CRI model, the ACCMIP members
 583 and their ENSEMBLE. Error bars indicate 2-sigma confidence limits for the observations
 584 and ACCMIP ENSEMBLE. The standard deviations of the results of the ACCMIP members are
 585 annotated for both amplitudes at the three sites.



586

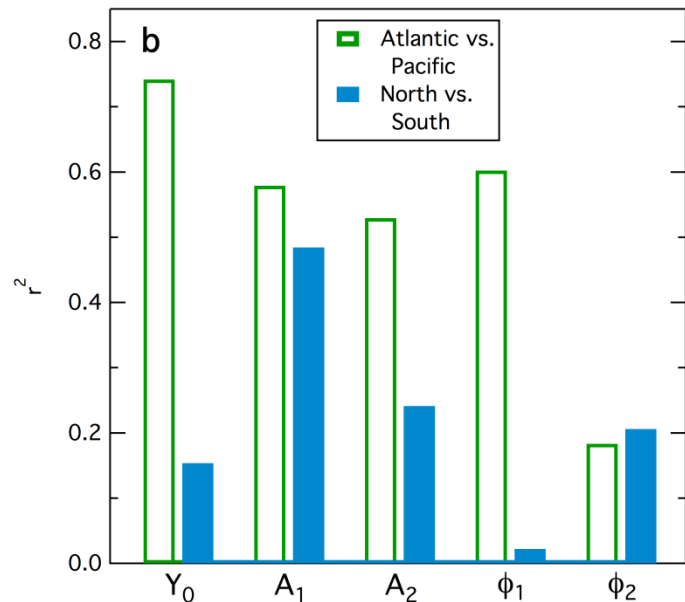
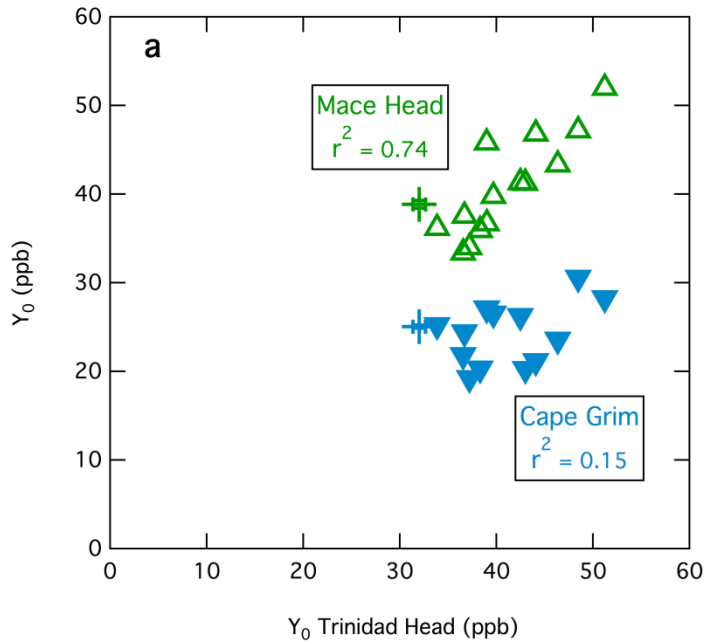
587 **Figure 4.** Comparison of the observed and model values of the fundamental and second
588 harmonic phase angles, ϕ_1 and ϕ_2 , in radians for the STOCHEM-CRI model, the ACCMIP
589 members and their ENSEMBLE. The ϕ_1 values for the northern hemisphere stations have
590 been shifted by $-\pi$ radians to allow direct comparison with the southern hemisphere station.
591 Error bars indicate 2-sigma confidence limits for the observations and ACCMIP ENSEMBLE.
592 The standard deviations of the results of the ACCMIP members are annotated for both
593 phase angles at the three stations.



595

596 **Figure 5.** Comparison of the observed and model values of the differences in Y_0 (ppb), the
 597 two amplitudes (ppb) and the two phase angles (months), for the STOICHEM-CRI model, the
 598 ACCMIP members and their ENSEMBLE. The differences are between the northern and
 599 southern hemispheres (calculated from Trinidad Head - Cape Grim) with ϕ_1 at Trinidad Head
 600 shifted by π radians so that a difference of 0 indicates both have the same seasonal cycle,
 601 but shifted by 6 months between hemispheres) and between the Atlantic and Pacific inflow
 602 (calculated from Mace Head - Trinidad Head). Error bars indicate 2-sigma confidence limits
 603 for the observations and ACCMIP ENSEMBLE. The standard deviations of the results of the
 604 ACCMIP members are annotated for all parameters at the three sites.

605



606

607 **Figure 6. a)** Correlation of Y_0 for Mace Head and Cape Grim with that for Trinidad Head.
 608 The triangles give the results derived by the fourteen ACCMIP members, and the plus
 609 symbols with error bars (smaller than the symbols) indicate the observations. The square of
 610 the linear correlation coefficient is annotated for each set of results. **b)** Comparison of the
 611 squares of the linear correlation coefficients for all five parameters derived from the
 612 fourteen ACCMIP members. The correlations are for North Atlantic versus North Pacific
 613 inflow (i.e., Mace Head versus Trinidad Head) and northern versus southern hemisphere
 614 (i.e., Cape Grim versus Trinidad Head).

615